BIOCHEMISTRY
including biophysical chemistry & molecular biology

Article

pubs.acs.org/biochemistry

The Protonation State of Catalytic Residues in the Resting State of KasA Revisited: Detailed Mechanism for the Activation of KasA by Its Own Substrate

Wook Lee and Bernd Engels*

Institut für Physikalische und Theoretische Chemie, Universität Würzburg, Emil-Fischer Strasse 42, 97074 Würzburg, Germany

Supporting Information

ABSTRACT: *Mycobacterium tuberculosis* is the causative pathogen of tuberculosis, the second leading cause of death from an infectious disease globally. β-Ketoacyl ACP synthase I (KasA) is essential for the survival of *M. tuberculosis*, because it is one of the key enzymes in the biosynthetic pathway of mycolic acid, the building block of the cell wall in *M. tuberculosis*. To distinguish among the various suggested mechanisms of KasA that are based on different protonation states of the active site, we characterize its resting state by various theoretical approaches ranging from first-principle-based quantum mechanical/molecular mechanical molecular dynamics simulations (QM/MM MD) with large QM parts to force field-based MD and free energy perturbation computations. In contrast to a previous study that used less reliable semiempirical approaches in combination with smaller QM parts, our improved computations predict that the most important active site residues, Cys171 and His311, are neutral. Because the neutral catalytic residues are too unreactive to attack the substrate, the question of how their activation is achieved arises. Combining our computed results with structural information about the malonyl binding pocket, we devised a detailed model about the activation mechanism. A conformational change of Phe404 possibly triggered by the substrate is central for the activation because it switches KasA to the sufficiently reactive zwitterionic state.

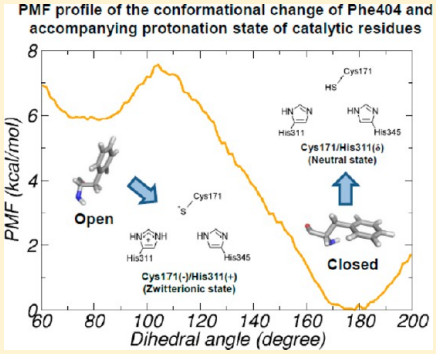

Tuberculosis (TB) is an infectious disease caused by *Mycobacterium tuberculosis*. According to the report from the World Health Organization in 2011, there were 8.5−9.2 million incident cases and 1.2−1.5 million deaths estimated in 2010, and this made TB the second leading cause of death from an infectious disease worldwide.[1] The emergence of multi-drug-resistant strains (MDR-TB) that acquire drug resistance to the two most commonly used front-line antituberculosis agents, isoniazid and rifampicin, made the treatment of TB far from trivial.[2] To make matters worse, the emergence of extensively drug-resistant strains (XDR-TB), which makes most of the known antibiotics for treating tuberculosis ineffective,[3] was further reported during the treatment of MDR-TB, and developing new drugs against tuberculosis became an urgent need.

Mycolic acids are very long-chain fatty acids that constitute the cell wall in mycobacteria. They provide many important characteristics such as resistance to chemical injuries[4] and dehydration,[5] biofilm formation,[6] acid-fast staining,[7] and the low permeability to hydrophobic antibiotics,[8] but most of all, they are very important for the ability of mycobacteria to persist within the host.[5,7,9,10] Thus, the synthesis of the mycolic acids is an indispensable part of the life of mycobacteria. The biosynthetic pathway of mycolic acids consists of two systems, namely, fatty acid synthesis (FAS) I and II. FAS I conducts *de novo* synthesis of fatty acids, and it is similar to the system found in mammals. It consists of a single gene that encodes a polypeptide containing all required enzymatic activities and carrier functions.[11] FAS II, which elongates the fatty acyl-CoA primers (C_{14-16}) generated by FAS I, is analogous to the system found in other bacteria, plants, and parasites but does not exist in mammals.[11] In contrast to FAS I, the enzymes involved in FAS II are encoded by separate genes and play distinctive roles.[12]

KasA catalyzes the reaction that condenses a long acyl chain and a malonyl residue, thereby elongating the original acyl chain further by two carbon units.[13] The importance of KasA for the survival of *M. tuberculosis* was demonstrated by the finding that its depletion leads to cell lysis.[14] It has a catalytic triad, namely, Cys171, His311, and His345. Its catalytic cycle comprises three steps (Scheme 1) and is initiated by the covalent transfer of an acyl group from an acyl carrier protein (ACP) to Cys171 (acylation step). After ACP has left the active site, another ACP carrying a malonyl group binds to the active site. Through the detachment of the terminal carboxylate group (decarboxylation step), a carbanion intermediate is generated. In the final condensation step, this carbanion attacks the carbonyl carbon of acylated Cys171, releasing an elongated acyl chain.

The role of other important conserved residues in KasA was also investigated by several experimental and computational

Received: September 20, 2013
Revised: January 7, 2014
Published: January 20, 2014

   dx.doi.org/10.1021/bi401308j | *Biochemistry* 2014, 53, 919−931

Scheme 1. Three Steps in the Catalytic Reaction of KasA

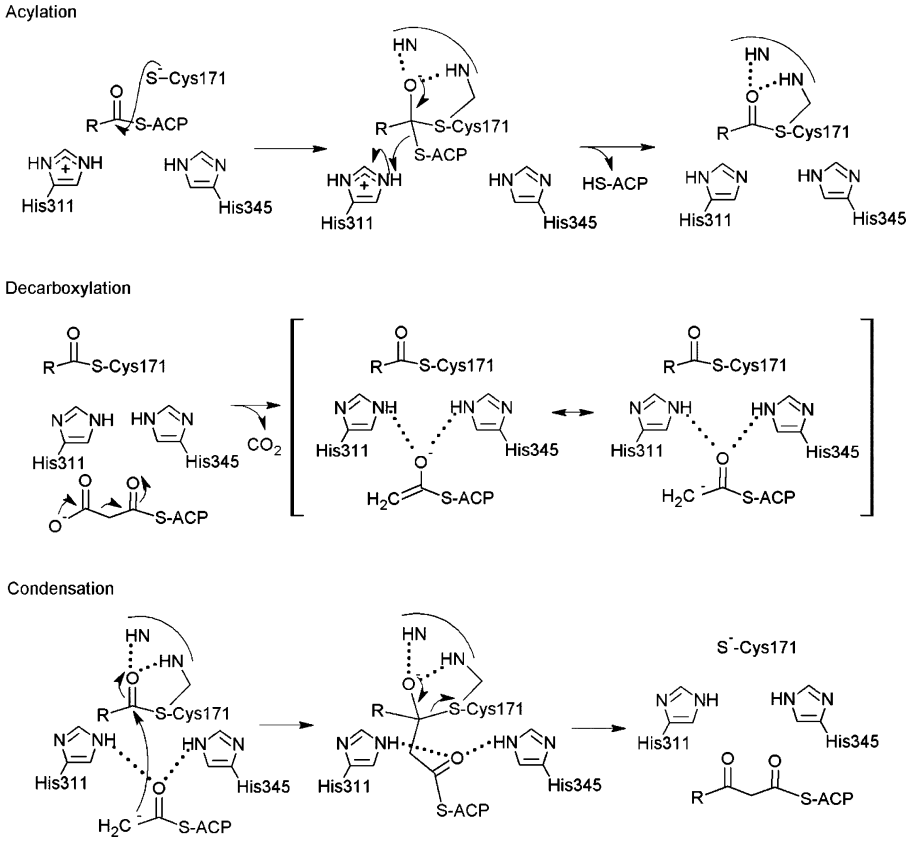

studies. Phe404, which is located directly above the catalytic Cys171, is assumed to function as a gatekeeper because the conformational change of its side chain is essential for an acyl substrate to gain full access to the catalytic Cys171.[15] The conformational flexibility resulting from neighboring conserved glycine residues, Gly403, Gly405, and Gly406, further underpins this assumption. The role of Phe404 as a gatekeeper was also addressed by Luckner et al.,[16] who determined X-ray crystal structures of wild-type KasA and its Cys171Gln mutant. The latter was reported to mimic the accompanying structural change by an acylation.[17] Comparing both structures, they suggested that Phe404 in the acyl-enzyme state of KasA can take an open conformation that facilitates the binding of the inhibitor thiolactomycin through the widening of the entrance of the malonyl binding pocket. The conserved residue Lys340 has also attracted attention. It was generally accepted that it is protonated and forms a stable salt bridge with the adjacent deprotonated Glu354 residue.[18−21] Many mutational studies showed that the substitution of Lys340 with alanine resulted in remarkably reduced catalytic activities.[20,22−24] On the basis of an X-ray crystal structure of this lysine mutant, it was suggested that the conserved lysine residue is important for maintaining the structure of the active site.[20]

Because of its three catalytic residues, Cys171, His311, and His345, the active site of KasA can formally take 18 different protonation states. Detailed knowledge of the actual protonation states is important for clarifying the catalytic reaction of KasA because proposed mechanisms differ in their protonation states. Because X-ray investigations could not provide unambiguous information about the protonation state in this case, we used theoretical approaches to shed some light on this important issue.[25,26] Our first study[25] was devoted to the protonation state of the resting state. We used force field-based MD simulations to compute the geometrical orientations of the various residues as a function of the protonation state. To determine relative energies between the various protonation states, we had to use QM/MM-based umbrella sampling because the relative energies computed from a static QM/MM optimization depend strongly on the starting structure. Because of the high level of computational effort, we could only employ semiempirical methods for the QM part. Furthermore, the Lys340/Glu354 pair was described within the MM part at that time. This seemed sufficiently accurate because it was generally assumed that the Lys340/Glu354 pair forms a stable salt bridge whose influence on the protonation state of the active site should be accurately taken into account through the MM treatment.[18−21] Mainly on the basis of comparisons of simulated structural properties with X-ray data, our first study came to the conclusion that KasA has a zwitterionic character (Scheme 2) in the resting state.[25] Furthermore, our QM/MM computations indicated that the relative energy difference between the neutral and zwitterionic state is nearly isoenergetic.

In our second study,[26] we investigated the protonation state of His311 in the acyl-enzyme state to determine which of the suggested mechanisms for decarboxylation step is correct. The results from density functional theory (DFT)-based QM/MM MD simulations and FEP computations indicated His311 to be protonated at N_ε in the acyl-enzyme state. On the basis of this finding, we supported the mechanism given in Scheme 1 to be the most probable catalytic cycle of KasA. These computations could contribute to the clarification of the catalytic cycle of KasA, but they questioned the finding of our first study. In contrast to our assumption that Lys340 and Glu354 form a stable zwitterionic salt bridge, the new computations indicated

dx.doi.org/10.1021/bi401308j | Biochemistry 2014, 53, 919−931

Scheme 2. Six Possible Protonation States of Catalytic Residues in KasA[a]

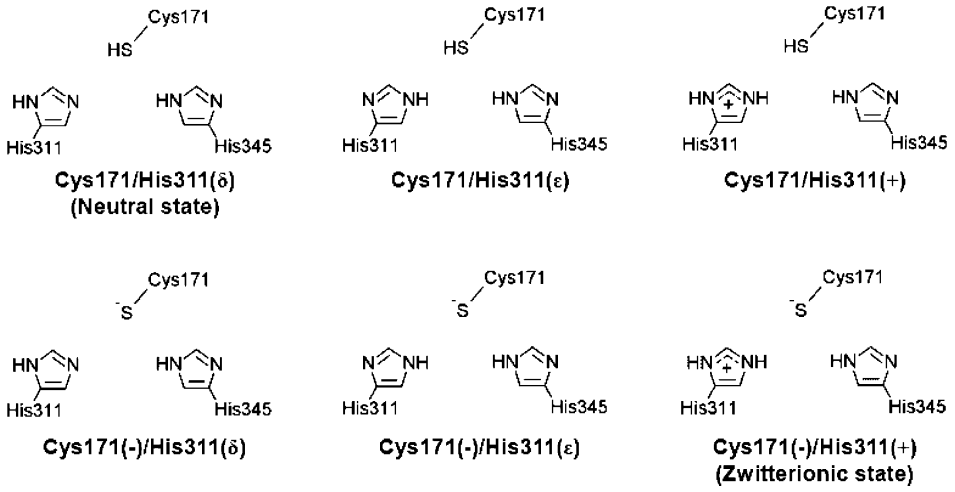

[a]A conserved water molecule positioned between Cys171 and His311 has been omitted for the sake of clarity.

a frequent proton hopping between constituting residues. As a consequence, the charge distribution of the Lys340/Glu354 pair varies between neutral and zwitterionic instead of being purely zwitterionic. This difference might of course influence the outcome of the simulations about the protonation state of the active site.

Because the protonation pattern within the resting state is of outmost importance for the development of new inhibitors, it is the first goal of this paper to determine if the variation in the character of the Lys340/Glu354 indeed influences the computed protonation state of the active site. In contrast to our first study, the new computations indeed predict a neutral resting state (Scheme 2). Because a neutral state is not sufficiently reactive to attack the substrate,[27] this leads to the question of how the enzyme is activated for the catalytic cycle. Simulations for answering this question represent the second goal of this paper. Answers to this question are achieved by combining our computations with structural information about the distribution of polar and nonpolar residues in the malonyl binding pocket. The results indicate that the enzyme is actually activated by the substrate. The third goal of this study is connected with the catalytic cycle (Scheme 1) proposed in our previous study. Because the protonation state of the active site after the catalytic cycle (last part of condensation step) differs from the protonation state at the beginning of the cycle (start of acylation step), the question of how KasA is able to change its protonation state arises.

The computations performed in this investigation were not possible when we conducted our first study.[25] This study includes the Lys340/Glu354 pair in the QM part to ensure an accurate description of its complicated electronic structure. Additionally, QM/MM MD is performed instead of static QM/MM minimization to describe the frequent proton transfers between the Lys340/Glu354 pair. Furthermore, because semiempirical approaches turned out to be too inaccurate,[28] we employed DFT approaches that were proven to be sufficiently accurate. Such computations have become feasible through the use of graphics processing unit (GPU) clusters and a developmental version of AMBER 11 in combination with Terachem (version 1.46-dev).[29,30] Both tools were not available for us when we conducted our first study. They allowed us to perform 100 ps of QM/MM MD simulations including all important residues in the QM part.

The paper is organized as follows. In the next section, we summarize the descriptions of the theoretical methods employed for the various computations. In the first part of the subsequent section, we discuss the new simulations about the protonation status of the active site. Their results provide an improved description of the protonation pattern of the active site in the resting state (first goal). By establishing an equilibrium between the respective protonation patterns, these results also indicate how the enzyme recovers at the end of the cycle (third goal). Finally, combining our computations with additional information about the residues in the active site, we speculate about the mechanism of how the enzyme is activated by the substrate (second goal).

METHODS

The initial structure for the various QM/MM MD simulations was taken from the X-ray crystal structure of wild-type KasA from *M. tuberculosis* [Protein Data Bank (PDB) entry 2WGD]. The protein was solvated in a water shell with a radius of 45 Å using the TIP3P water model,[31] and the system was neutralized by adding a total of 29−30 sodium ions employing the leap module in AMBERTOOLS version 1.4. Using the sander module of AMBER 11[32] in combination with the ff99SB parameter set,[33] the solvated and neutralized system was subsequently energy minimized for 500 steps to relax steric clashes. Subsequently, the system was gradually heated from 50 to 310 K employing positional restraints on the protein. The restraints were gradually decreased to zero once the temperature reached 310 K. For the final preparation, the system was equilibrated for more than 50 ps. These preparation steps were conducted at the MM level, and a spherical boundary condition was applied.

In static QM/MM computations, the chosen reaction coordinate is varied while all other degrees of freedom are relaxed for a given value of the reaction coordinate. In a QM/MM MD simulation for a given restrained value of the reaction coordinate, an MD simulation is performed for all other degrees of freedom. This allows the computation of free energies instead of enthalpies. Further differences arise because the relaxation performed in the static QM/MM computation leads the system only to the next local minima. On the other hand, during the

dx.doi.org/10.1021/bi401308j | *Biochemistry* 2014, 53, 919−931

MD run performed with the QM/MM MD simulations, the system can surmount energy barriers so that lower-lying minima become accessible. Often the second effect is larger than the first. In this work, the QM/MM MD simulations were performed with the developmental version of AMBER 11 in combination with Terachem (version 1.46-dev).[29,30] Time steps of 1 fs were used for those simulations, and the cutoff value of 18 Å was employed for nonbonded interactions. To maintain the temperature constant during simulations, a Langevin thermostat was used. The Becke−Lee−Yang−Parr (BLYP) exchange-correlation functional[34−36] in combination with the 6-31G**[37−40] basis set was employed for the QM part because semiempirical methods were shown to lead to severe errors.[28] Dispersion interaction was taken into account via Grimme's correction scheme.[41] For the MM part, we used the AMBER ff99SB force field parameter set. For the various questions, we used QM parts of different sizes. For the amino acids included in the QM part, the boundaries were set at the bond between the α- and β-carbons of cysteines and histidines, the β- and γ-carbons of glutamates, and the δ- and ε-carbons of lysines.

Because of a computational cost, only the BLYP/6-31G** level of theory was feasible. This approach was already successfully adopted in a large number of theoretical studies[42−50] and also gave results comparable to those of LCCSD(T)/cc-pVQZ in our recent benchmark study for the transfer of a proton between Lys340 and Glu354.[26] Further insights into the accuracy for these questions are offered in Table 1, which compares computed energy differences for the transfer of a proton between Cys171 and His311 via a water molecule. The COSMO approach[51] was used to simulate environmental effects. According to these results, BLYP/6-31G** is in excellent agreement with the SCS-MP2/aug-cc-pVTZ approach. The high accuracy of SCS-MP2/aug-cc-pVTZ was proven in a recent benchmark paper.[28] These computations were conducted using the Turbomole program package.[52]

Table 1. Benchmark Computation Results for the Energy Difference (ΔE) between the Zwitterionic [Cys171(−)/His311(+)] and Neutral [Cys171/His311(δ)] States

level of theory	ΔE (kcal/mol)
BLYP/6-31G**	3.6
BLYP/6-311G**	2.0
BLYP/6-311++G**	3.4
SCS-MP2/cc-pVTZ	4.8
SCS-MP2/aug-cc-pVTZ	3.4

To gain insights into the structural changes in the active site upon substrate binding, a force field-based MD simulation was performed for a tetrahedral intermediate state. The initial structure of the tetrahedral intermediate was built manually using MOLDEN[53] and then optimized at the B3LYP/TZVP level of theory. The electrostatic potential of this optimized structure was further computed by HF/6-31G*. These calculations were conducted using Gaussian03.[54] Subsequently, partial charges were fit from the computed electrostatic potential using the restrained electrostatic potential (RESP) method.[55] Because the force field parameters for the tetrahedral intermediate are not available in the ff99SB parameter set, they were taken from the General AMBER force field[56] (GAFF) and assigned by antechamber.[57] The X-ray crystal structure of the Cys171Gln mutant complexed with the inhibitor thiolactomycin (PDB entry 2WGG) was used as a starting structure for creating this model system. The inhibitor was removed from the active site, and Gln171 was modified into the tetrahedral intermediate. The heating and the equilibration were conducted as described above. For the 1 ns productive run, we used the same conditions used for the other MD simulations. The reliability of GAFF in describing the tetrahedral intermediate was also investigated (see the Supporting Information).

To compute the pK_a values of His311 with the alchemical FEP method,[58] we employed the NAMD version 2.7 simulation package[59] in combination with the CHARMM 22 force field[60] with CMAP corrections.[61] The preparation of model systems and simulation conditions were identical to those of all other MD simulations, but a time step of 2 fs was used in combination with a RATTLE algorithm[62] to constrain the bonds including hydrogen atoms. As reference systems for the thermodynamic cycle, we used a single histidine residue. Both termini were capped with a neutral blocking group, and the capped histidine was solvated in a water shell with a radius of 22 Å. The alchemical transformation was stratified into 100 windows with an even width. The dual-topology paradigm was adopted. For each window, we performed a 15 ps simulation for equilibration and a 40 ps simulation for the productive run. Soft core potentials were employed to avoid end-point catastrophe.[63−65] Each FEP computation was repeated four times to address the accuracy of the computations,[66,67] and the analysis to evaluate the convergence of this computation was also performed (see the Supporting Information). A harmonic restraint was applied to the model systems with the neutral Lys340/Glu354 pair to maintain their hydrogen bond, thereby preventing a collapse of the hydrogen bond network. This problem was not observed in the model systems with an ionic Lys340/Glu354 pair. Unlike other computations, the CHARMM force field was used in FEP computations because of the technical difficulties in employing the AMBER force field for FEP computations implemented in NAMD. However, this would not affect the consistency of the calculations because these FEP computations are completely independent of other computations.

The potential of mean force (PMF) profile for the conformational change of Phe404 was obtained by umbrella samplings using again Amber force field ff99SB in combination with the same conditions mentioned above. Each window consists of a 50 ps equilibration and a 50 ps productive run. The PMF profile was computed with the weighted histogram analysis method (WHAM)[68−70] as implemented in the software developed by Grossfield.[71]

RESULTS AND DISCUSSION

Protonation State in the Resting State and Recovery at the End of the Catalytic Cycle. KasA has three catalytic residues, namely, Cys171, His311, and His345, which formally can take 18 different protonation states. In these possibilities, states with negatively charged histidines were not considered. His345 is expected to be N_ε-protonated because many X-ray structures show that its N_δ accepts a hydrogen bond from the backbone amide of Ile347. These considerations reduce the number of possible states to six, which are depicted in Scheme 2. From these states, protonation states Cys171/His311(ε) and Cys171/His311(+) can also be ruled out because they are not able to attack the substrate. As a result, the protonation states we have to actually consider can be narrowed down to four.

Mainly on the basis of structural arguments but also supported by a semiempirically based PMF surface, we recently

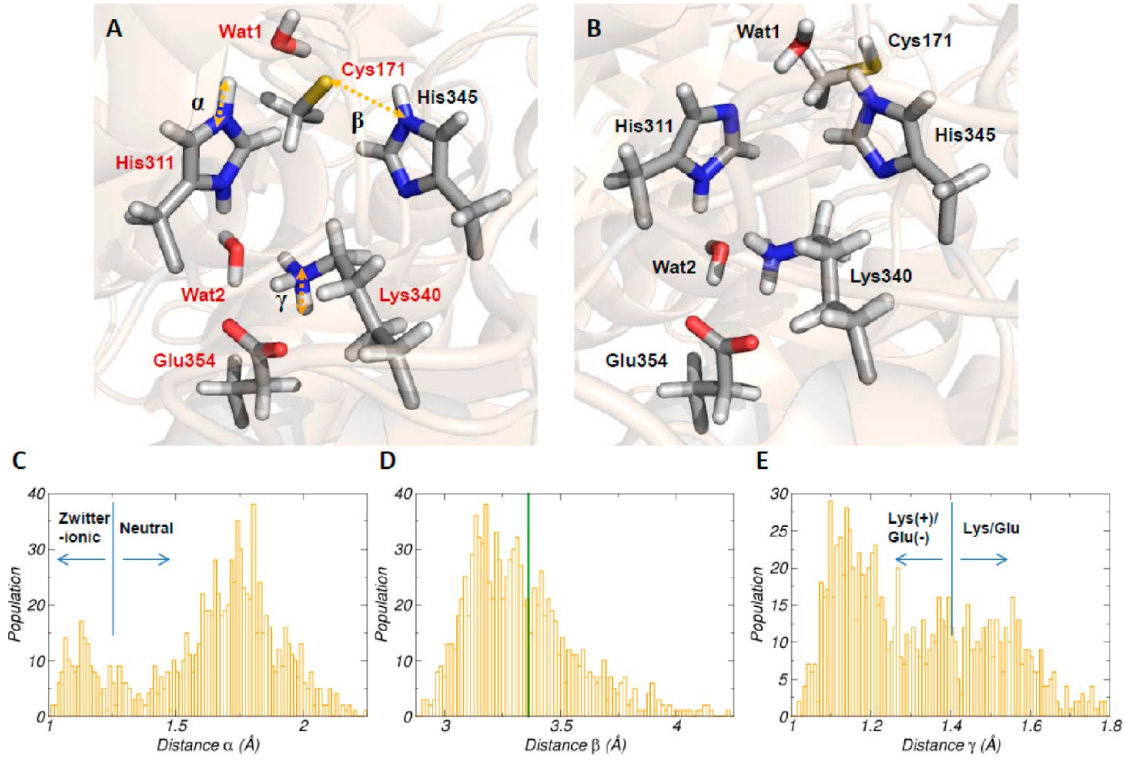

Figure 1. Distributions of the distances of interest in the resting state. Panels A and B show representative frames from the force field-based MD simulation of the zwitterionic state and the neutral state, respectively. The name of residues involved in the QM region during QM/MM MD is shown in red in panel A. The corresponding distributions for the distances marked α, β, and γ in panel A are shown in panels C–E, respectively.

predicted the zwitterionic state [Cys171(−)/His311(+)] to be the most probable protonation state in the resting state,[25] but this seems to be questionable in light of newer simulations.[26,28] They showed that the employed semiempirical method artificially favors the zwitterionic state with respect to its neutral counterpart[28] and that the electronic character of the Lys340/Glu354 pair is not purely ionic as generally accepted at that time.[26] To come to more reliable estimates about the protonation state of the catalytic residues in the resting state of KasA, we used more accurate DFT ansatz (BLYP/6-31G**) for the QM part and performed a 100 ps QM/MM MD simulation for the zwitterionic state to take into account the possible proton hopping between the constituent residues. The QM part (Figure 1A) comprises Cys171, His311, the bridging water molecule (Wat1), Lys340, and Glu354. The conserved Wat2 was also added to the QM part to account for possible transfers of protons from His311 to Glu354 via Wat2. In this QM/MM MD simulation, we did not constrain any internal coordinate; i.e., all atoms can freely move. The simulation took nearly a month. Hence, the computation of an accurate energy profile that would require this computation to be repeated ≥50 times is too demanding despite the new available hardware and software. However, the population of both the neutral and zwitterionic states still can be estimated from the distribution of the positions of the transferred proton during QM/MM MD simulations. Figure 1C shows the corresponding histogram that monitors the position of the proton along distance α (Figure 1A). Fortunately, because of the small energy barriers, the proton hops so often during the simulations that the data are statistically valid. The duration of the simulation (100 ps) also seems to be sufficient for our purpose because the motion of the side chains of amino acids or proton transfers takes place on the picosecond or even lower time scale. Figure 1C indicates that the neutral state is considerably more populated than the zwitterionic state; i.e., the catalytic residues are predicted to prefer the neutral rather than the zwitterionic state.

Our previous prediction about the protonation pattern of the resting state was mainly based on the orientation of His345 (Figure 1A,B), which could be compared with the X-ray crystal structure (PDB entry 2WGD).[25] In the force field-based simulations performed at that time, His345 pointed to the sulfur center of Cys171 in the zwitterionic state (Figure 1A), which resembles the X-ray crystal structure. In contrast, His345 pointed toward the oxygen center of Wat1 in the neutral state (Figure 1B), which differs considerably from the X-ray information. However, in this study in which all involved residues are treated quantum mechanically, this difference disappears. This is indicated in Figure 1D that plots distance β (Figure 1A) from the trajectory of the corresponding QM/MM MD simulation in comparison to the value taken from the X-ray crystal structure (green vertical line). The distribution of distance γ (Figure 1E) gives information about the preferred protonation state of the Lys340/Glu354 pair, and our computations show that both states are similarly populated, indicating the small energy difference between both states.

The QM/MM MD simulation discussed so far cannot compare the neutral state with the Cys171(−)/His311(δ) and Cys171(−)/His311(ε) states because the number of protons differs (Scheme 2). In our previous force field-based simulations, we excluded Cys171(−)/His311(ε) because the computed distribution of distance δ (Figure 2A) did not agree with the X-ray data. In the X-ray crystal structure, the distance between the oxygen center of Wat2 and N_δ of His311 is in the range of hydrogen bond formation (2.78 Å); however, this hydrogen bond was not observed in the previous force field-based simulation of Cys171(−)/His311(ε), and Wat2 took the

dx.doi.org/10.1021/bi401308j | *Biochemistry* 2014, 53, 919–931

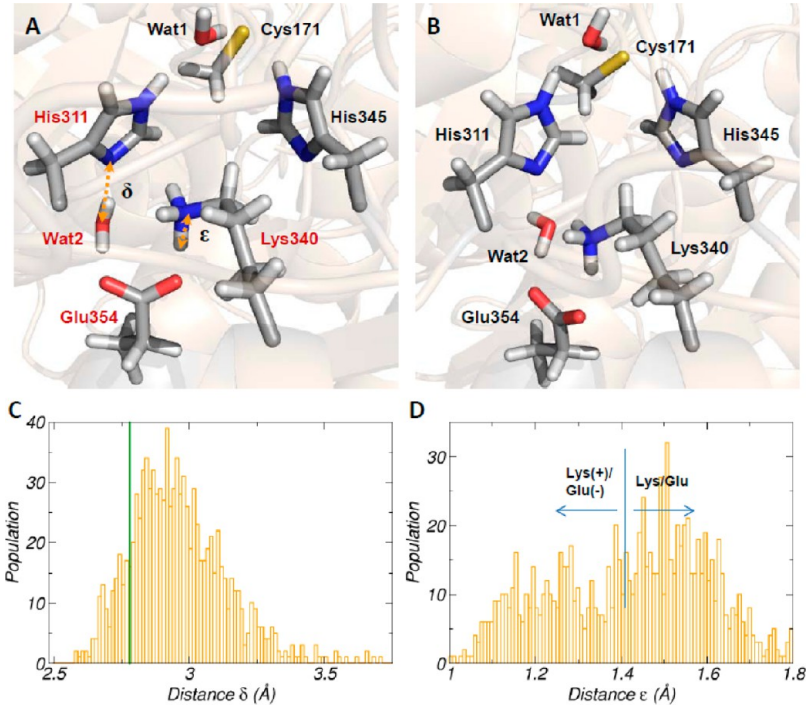

Figure 2. Distributions of the distances of interest in the system with protonation state Cys171(−)/His311(ε). Panel A shows a representative frame from QM/MM MD, and panel B shows a representative frame from force field-based MD. The names of residues involved in the QM region during QM/MM MD are shown in red in panel A. The corresponding distributions for the distances marked as δ and ε in panel A are shown in panels C and D, respectively.

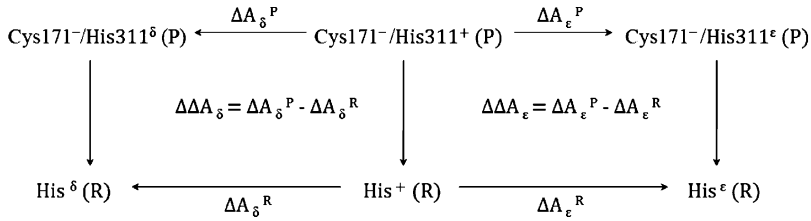

Figure 3. Thermodynamic cycles devised to compute pK_a values at both protonation sites of His311. (P) represents the protein environment, and (R) represents the reference system in which simulations are performed in the water shell.

orientation as shown in Figure 2B. To exclude errors arising from the shortcomings discussed earlier, we also performed improved QM/MM MD simulation for this state. In these computations, the QM part included residues His311, Lys340, and Glu354, and the bridging Wat2. Residue Cys171 and Wat1 were excluded from the QM part to ensure that Cys171 remains to be deprotonated.

In our improved QM/MM MD description, Wat2 is observed to form a hydrogen bond with N_δ of His311 (Figure 2A). Because the distribution of distance δ shows a peak in the vicinity of the experimental value (green vertical line in Figure 2C), the new simulations do not exclude protonation state Cys171(−)/His311(ε). Figure 2D, which analyzes the bonding character of the Lys340/Glu354 pair by monitoring distance ε in Figure 2A, indicates again the mixed zwitterionic and neutral character of the Lys340/Glu354 pair.

The Cys171(−)/His311(δ) and Cys171(−)/His311(ε) states cannot be directly compared to the neutral state but can be connected to the Cys171(−)/His311(+) zwitterionic state via force field-based FEP simulations. The corresponding thermodynamic cycles are shown in Figure 3. The processes in the upper horizontal connections represent alchemical transformations from doubly protonated His311 to either the N_δ-protonated (left side of Figure 3) or N_ε-protonated His311 (right side of Figure 3) in the protein environment. The bottom part represents the corresponding alchemical transformations in the water shell. Because these FEP simulations were force field-based, the calculations were performed separately for the neutral or ionic Lys340/Glu354 pair as extreme cases. The computed free energy differences together with the derived pK_a values are listed in Table 2.

For N_ε of His311, the computations predict pK_a values of around 10 and 13.4 for an ionic and a neutral Lys340/Glue354 pair, respectively. For N_δ of His311, the corresponding values are 6.5 and 8.7, respectively. The considerably higher acidity of the N_δ center rules out the Cys171(−)/His311(δ) state as a possible protonation state; i.e., the N_ε center is supposed to be always protonated. The computed pK_a values of N_δ also indicate an equilibrium between Cys171(−)/His311(ε) and the zwitterionic state for an environment with a pH of 7. Depending on the protonation state of the Lys340/Glu354 state, the ratio between the zwitterionic state and Cys171(−)/His311(ε) in this equilibrium varies between 32:68 and 98:2. The results of our computations described so far are summarized in Scheme 3. The FEP simulations predict an equilibrium between Cys171(−)/His311(ε) and the zwitterionic

dx.doi.org/10.1021/bi401308j | *Biochemistry* 2014, 53, 919−931

Table 2. Computed Free Energies and Derived pK_a Values for Both Protonation Sites of His311[a]

	Lys340(+)/Glu354(−)		Lys340/Glu354	
	N_δ position	N_ε position	N_δ position	N_ε position
ΔA^P	38.0 ± 1.7	43.9 ± 1.0	41.1 ± 1.1	48.6 ± 0.6
ΔA^R	37.3 ± 0.8[b]	38.1 ± 1.0[b]	37.3 ± 0.8[b]	38.1 ± 1.0[b]
$\Delta\Delta A$	0.7 ± 1.9	5.8 ± 1.4	3.8 ± 1.4	10.5 ± 1.2
pK_a	6.5	10.1	8.7	13.4

[a]All energies are given in kilocalories per mole. [b]These values are taken from ref 26.

state. Additionally, our QM/MM MD simulations predict that the zwitterionic state is less populated than the neutral state. When both results are combined, the enzyme is predicted to mainly populate the neutral state in its resting state. According to our previous computations,[26] the catalytic cycle ends in protonation state Cys171(−)/His311(ε) (Scheme 1), while the neutral state is mainly populated in the resting state according to our results. The equilibrium indicated in Scheme 3 explains this recovery of the active site in the enzyme at the end of the catalytic cycle, i.e., the transfer from Cys171(−)/His311(ε) to the neutral state taking place via the zwitterionic state.

Detailed Mechanism about the Activation of KasA. The results obtained so far suggest answers to the question about the protonation pattern in the resting state (neutral), and how the enzyme recovers at the end of the catalytic cycle (equilibrium given in Scheme 3). However, because the thiol group of Cys171 was found to be too unreactive for a reaction with carbonyl groups,[27] this raises the question of how the enzyme is activated. The reaction could take place because of the equilibrium between the neutral and zwitterionic state, but this is unexpected when the high efficiency of enzymes is taken into account. Hints about an alternative mechanism came from the observation that the His303Ala mutant of FabF (His311Ala in KasA) retains its acyl transfer activity.[23] Because of the mutation of His311, this activity cannot result from the zwitterionic state but relies solely on a cysteine residue that cannot transfer its proton to an accepting partner. Our previous simulation[25] explained this unexpected reactivity of Cys171 by the formation of a strong hydrogen bond between the sulfur center of Cys171 and the backbone amide of Phe404, and this bond is induced by the rotation of the aromatic ring of Phe404. Through the accompanying stabilization of the emerging thiolate, this hydrogen bond considerably increases the acidity of the thiol group so that Cys171 is predicted to be deprotonated in the resting state. In the wild type, this hydrogen bond is much weaker because the steric demands of His311 restrict the orientation of Phe404. In the His311Ala mutant, the smaller size of the alanine allows the rotation of Phe404 to the stabilizing position.

On the basis of these earlier results, here we hypothesize that the neutral catalytic residues could be activated by the same conformational change of Phe404 observed in the simulation of the His311Ala mutant. We will refer to this conformation as an "open" conformation because Cys171 becomes fully accessible in this conformation. To test whether this conformational change is energetically feasible, we computed the corresponding PMF profile using force field-based umbrella sampling. The computed profile is given in Figure 4D, which also sketches the rotation of Phe404. The closed form that is equivalent to the X-ray crystal structure of wild-type KasA (PDB entry 2WGD) is depicted in Figure 4A, while the geometrical arrangement of the computed open conformation is indicated in Figure 4C. The energy barrier for this rotation is computed to be 7−8 kcal/mol, while the relative energy difference between the open and closed conformation is predicted to be ∼6 kcal/mol. Both values are certainly in the range of enzymatic activation barriers. Additionally, the fact that the local minimum exists at the point that exactly corresponds to our suggested open conformation also implies that this open conformation is not an artifact but an intrinsic property of KasA.

To test whether KasA indeed becomes activated by the open conformation of Phe404, we conducted the same QM/MM MD simulation that was employed at the beginning of the study for the transfer of a proton between Cys171 and His311. However, we restricted Phe404 to its open conformation with a harmonic restraint at this time. To determine if the zwitterionic or neutral state is populated at a given point of the MD simulation, we monitored the distance between the transferred proton and N_ε of His311 (marked as ζ in Figure 4C). The computed distribution (Figure 4E) indicates that, in the open conformation, the catalytic residues indeed exclusively populate the zwitterionic state. The remarkable difference from the distribution obtained for the closed conformation (Figure 1C) implies that the conformational change of Phe404 undoubtedly causes a switch from the neutral state to the zwitterionic state of the catalytic residues. The formation of a strong hydrogen bond between the backbone amide of Phe404 and the sulfur center of Cys171 is demonstrated by the average bond length between both centers. It decreases from 2.73 Å for the closed conformation to 2.37 Å for the open conformation. The formation of this strong hydrogen bond in the open conformation of Phe404 can be explained by the interactions between Phe210 and Phe404. In the closed conformation, Phe210 and Phe404 are within van der Waals distance, and Phe210 pushes Phe404 from above so that the backbone amide of Phe404 is moved away from Cys171 (red arrows in Figure 4A). Such interactions are missing in the open conformation. Hence, the backbone amide of Phe404 can move closer to Cys171 (blue arrows in Figure 4C). Please note that the water molecule (Wat1) mediating the proton transfer is also involved in the stabilization.

On the basis of the X-ray crystal structure of the Cys171Gln mutant (PDB entry 2WGG), Luckner et al. also suggested an open conformation of Phe404 in KasA (Figure 4B).[16] However,

Scheme 3. Schematic Drawing Showing the Shift between Species of Interest

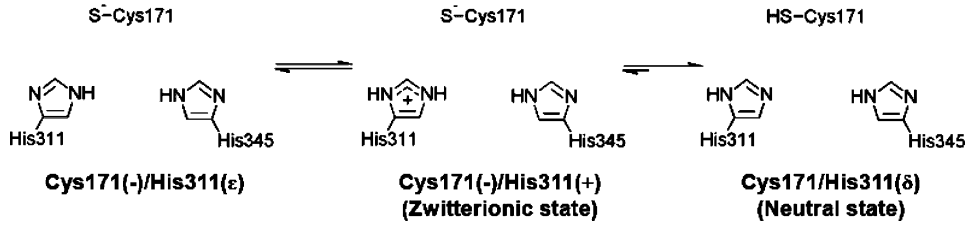

dx.doi.org/10.1021/bi401308j | Biochemistry 2014, 53, 919−931

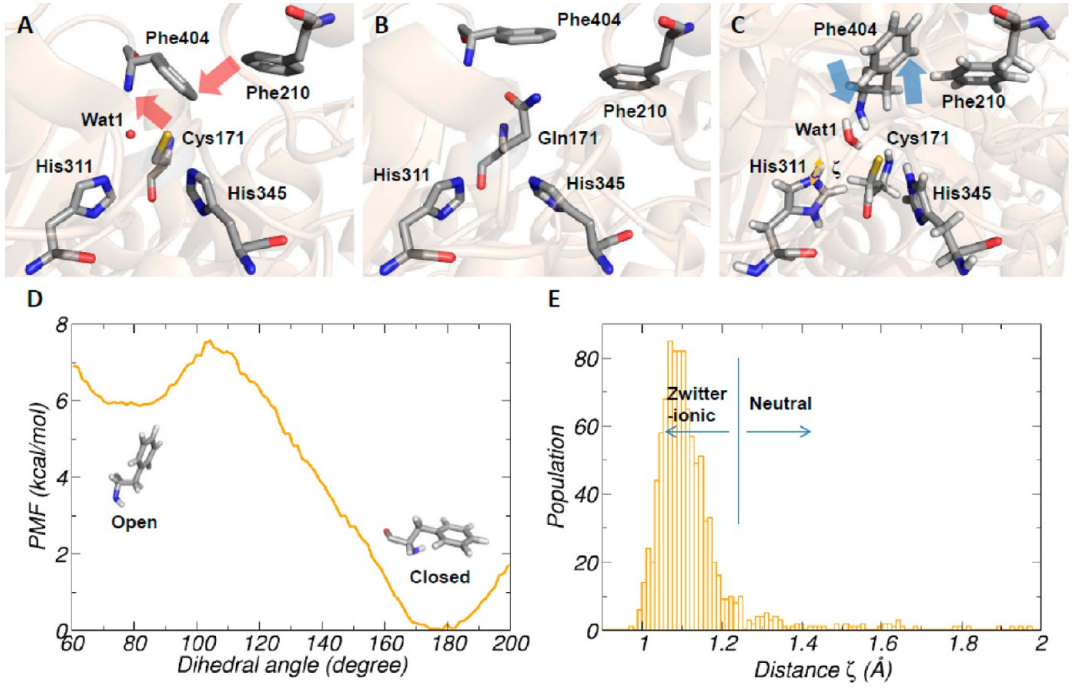

Figure 4. PMF profile along the rotation of the aromatic ring of Phe404 illustrating the switch from the closed to open conformation (D) and the distribution of the distances to evaluate the ratio between the populations of the neutral and zwitterionic state (E). Panels A and B were created from X-ray crystal structures (PDB entries 2WGD and 2WGG for panels A and B, respectively), and panel C was created from our simulation. The distribution of the distance marked as ζ in panel C is shown in panel E.

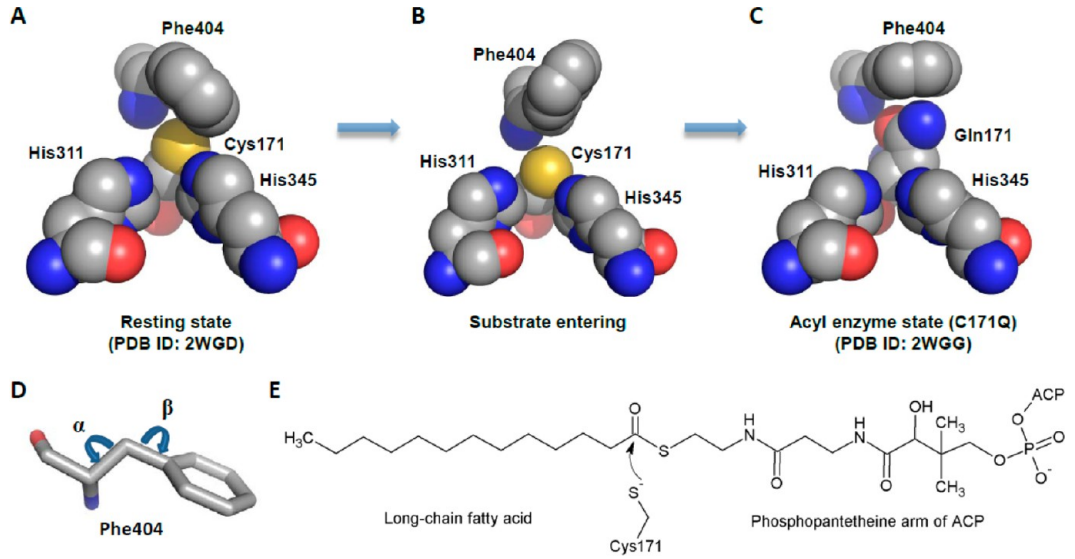

Figure 5. Putative series of conformational changes that occurred in Phe404 during the acyl transfer reaction and the chemical structure of the substrate. The residues in panels A–C are represented as their van der Waals radii. Panels A and C were created from X-ray crystal structures, and panel B was created from our simulation. The possible axes of rotation for conformational changes of Phe404 are shown in panel D. The chemical structure of an acyl substrate and the nucleophilic attack of Cys171 on it are shown in panel E.

this conformation deviates from the one predicted by our computations (Figure 4C). Figure 5, which sketches the involved residues with their van der Waals radii, compares those different conformations. The open conformation suggested by Luckner et al. (Figure 5C) is assumed to represent the acyl-enzyme state, while ours (Figure 5B) is expected to resemble the state before an acyl transfer reaction takes place. Luckner et al. used the term open because they observed that the corresponding conformational change widens the entrance of the malonyl binding pocket in the acyl-enzyme state compared to the resting state. On the other hand, our open conformation is devised for the acyl substrate to gain full access to the catalytic Cys171 at the beginning of the reaction. This is clearly indicated when comparing Figure 5A (closed conformation) to Figure 5B (open conformation). From Figure 5C, it is also obvious that the open conformation of Luckner et al. cannot provide sufficient space above Cys171 for an acyl substrate (Figure 5E), while this space would be available in the conformation predicted by our computations (Figure 5B). The difference between two conformations originates from the rotational

dx.doi.org/10.1021/bi401308j | *Biochemistry* 2014, 53, 919–931

axes (Figure 5D). The open conformation suggested by our computations is obtained through a rotation of the aromatic ring around axis α, while the open conformation suggested by Luckner et al. is achieved by a rotation around axis β.

The X-ray crystal structure of the wild type further supports our hypothesis. In the case of the wild type, the aromatic ring of Phe404 is below Phe210 (Figure 4A), while it is the other way around in the Cys171Gln mutant (Figure 4B). Assuming that the X-ray crystal structure of the Cys171Gln mutant correctly reflects the accompanying structural change by an acylation,[17] the movement of the aromatic ring of Phe404 from below to above Phe210 has to be feasible in the resting state. By the rotation around axis α, Phe404 can easily shift its aromatic ring from below to above Phe210. However, as observed in restrained MD simulations (data not shown), this cannot be achieved via a rotation around axis β because of the steric hindrance between Phe210 and Phe404.

In a widely accepted mechanism, the cysteine residues are activated by helix macro dipoles that especially stabilize the emerging thiolate at the N-terminus. In contrast, recent investigations employing first-principles-based QM/MM computations revealed a minor contribution of the helix macro dipoles in stabilizing the emerging thiolate.[72] The charge deletion analysis performed for KasA in our earlier work also supports this conclusion,[25] so that the activation mechanism based on the helix macro dipoles can be excluded. The activation could also result from a concerted mechanism in which the transfer of a proton from Cys171 to His311 takes place simultaneously with the nucleophilic attack of Cys171 on the substrate. This type of activation has been reported for serine hydrolase and protease.[73,74] Such a mechanism can also be easily conceived for KasA because our QM/MM MD results indicate a very low activation barrier for the proton transfer. However, unlike that of serine hydrolase or protease, the proton transfer between the catalytic residues is mediated by a bridging water molecule in KasA. This means that the proton transfer cannot take place if the substrate shoves aside the water molecule by entering the active site in advance of the reaction.

Insights into such effects would be provided by the simulations of an enzyme−substrate complex, but the indispensable structural information is missing. Because the substrates are expected to change their positions only slightly during the formation of the bond between Cys171 of the enzyme and the carbonyl carbon of the substrate, simulation of the tetrahedral intermediate of the acylation step (Scheme 1) also offers some information. We performed a 1 ns force field-based MD simulation for the tetrahedral intermediate state approximating the long-chain fatty acid and the phosphopantetheine arm of the substrate by a methyl group. Figure 6 compares a representative frame from the simulation with the neutral resting state. It shows that the thioester group connected to the phosphopantetheine arm occupies the same region of the active site that the bridging water molecule (Wat1) occupies in the resting state. This indicates that the water molecule will be pushed away from the active site before the reaction takes place, so the activation in a concerted manner seems unfeasible in KasA.

Combining our results with the positions of the conserved residues in the malonyl binding pocket of KasA (Figure 7), we can provide some new insights into the mechanism for the formation of the KasA−substrate complex and the activation of KasA. Considering the connecting point where ACP is attached in the acyl substrate (Figure 5E), it would enter the active site through the malonyl binding pocket, and the long-chain fatty

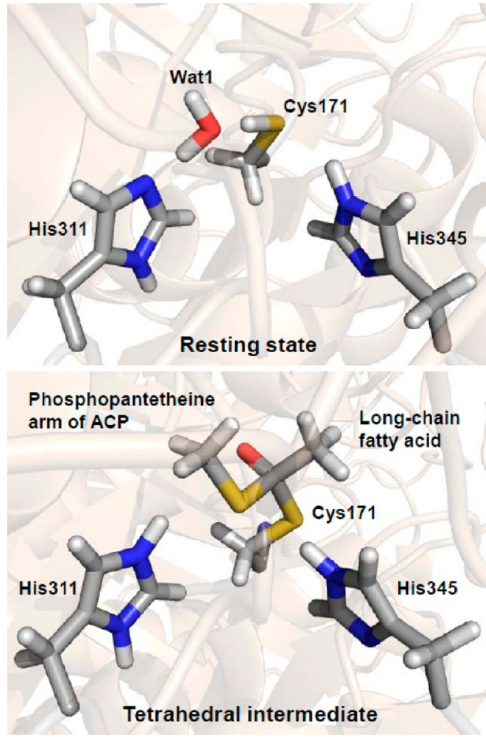

Figure 6. Comparison between the resting and tetrahedral intermediate states. The resting state is assumed to be neutral here.

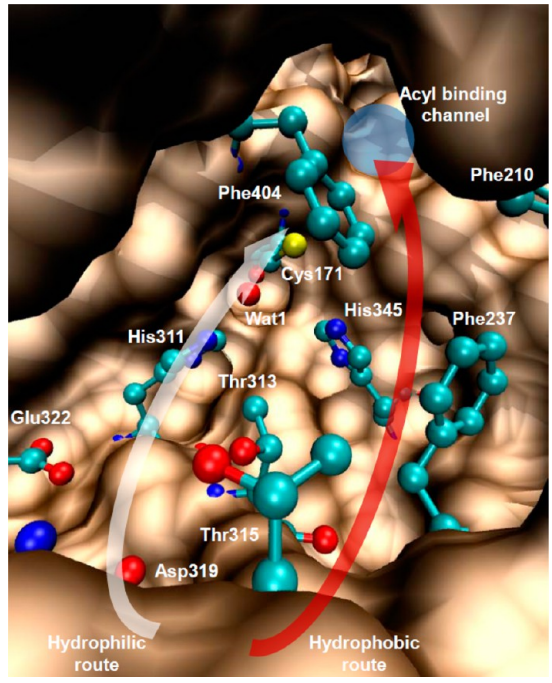

Figure 7. Malonyl binding pocket and conserved residues therein. All residues shown here are conserved. The location of an acyl binding channel is marked with a blue circle. The hydrophilic and hydrophobic routes are shown with white and red arrows, respectively.

acid of the substrate is supposed to enter first. When the substrate fully binds to the enzyme, the fatty acid is expected to be accommodated in the acyl binding channel that is located behind Cys171 (blue circle in Figure 7).[16] The various steps between those points are less known. Important information about this process comes from the distribution of conserved

dx.doi.org/10.1021/bi401308j | *Biochemistry* 2014, 53, 919−931

hydrophilic and hydrophobic residues in the malonyl binding pocket (Figure 7). The left side of the pocket contains only hydrophilic residues, while hydrophobic residues appear only in the right side of the pocket. Two conserved threonine residues comprise the borderline, laying their hydroxyl group on the hydrophilic side and the methyl group on the hydrophobic side. Because of this distribution, the malonyl binding pocket provides a hydrophobic (red arrow in Figure 7) and hydrophilic (white arrow in Figure 7) route. With the long-chain fatty acid (hydrophobic) and the phosphopantetheine arm (hydrophilic), the substrate also is divided into two parts with different electrostatics.

This suggests the following course of activation. The long-chain fatty acid that enters the malonyl binding pocket first takes the hydrophobic route. The catalytic residues, Cys171 and His311, are supposed to be neutral at this stage, and because the hydrophobic route is far from bridging water molecule Wat1, it can keep its bridging position. When the fatty acid reaches the entrance of the acyl binding channel, it pushes up Phe404 to the open conformation to enter the channel. The open conformation of Phe404 in turn promotes the transfer of a proton from Cys171 to His311 so that the catalytic residues become activated. At this point, the emerging thiolate, which is found to be very reactive in its isolated form, is stabilized through the hydrogen bond network consisting of the positively charged His311 via Wat1, the neutral His345, and the backbone amides of Cys171 and Phe404. Subsequently, the long-chain fatty acid starts to be accommodated in the acyl binding channel, and simultaneously, the phosphopantetheine arm starts to enter the active site along the hydrophilic route.

In the following step, the reactivity of the thiolate can be increased through a destruction of the stabilizing hydrogen bond network. The water molecule, Wat1, that is positioned on the hydrophilic route is expected to be pushed away by the phosphopantetheine arm of the substrate. According to the MD simulation results for the tetrahedral intermediate (Figure 6), His311 is expected to form a hydrogen bond to the sulfur center of the thioester group of the phosphopantetheine arm. This would predetermine the direction of the proton transfer, i.e., from the protonated His311 to the leaving ACP (Scheme 1), thereby facilitating the dissociation of the thiol group at the end of the acylation step. Finally, after the long-chain fatty acid is completely accommodated in the acyl binding channel, Phe404 possibly turns back to the closed conformation so that its stabilizing hydrogen bond to the thiolate is also weakened. The accompanying increase in the reactivity of the thiolate would in turn promote the attack on the substrate that is now in the right position for the reaction. This complicated mechanism, which relies on an active manipulation of the electronic structure of the active site through the substrate, also nicely explains the high specificity of KasA and why KasA is able to catalyze only elongated fatty acids and cannot contribute to the *de novo* synthesis.

Our work also can add some information to the design of improved inhibitors. Predicting the resting state of KasA to be neutral, we fully support the work of Sotriffer and co-workers,[75] who offered a suggestion for the inhibitor design based on MD simulations for the neutral state. For the design of covalent inhibitors, the role of Phe404 for the shift to the zwitterionic state is important. Because such inhibitors can react with only the zwitterionic state, they need a component that can induce the open conformation of Phe404 described in Figure 4C. As in the substrate, this component should be nonpolar, while the reacting electrophilic warhead, which is supposed to react with the thiolate, should possess polar groups. They will guide the warhead along the hydrophilic route so that it can push away the bridging water molecule, thereby destroying the stabilizing hydrogen bond network of the thiolate. For binding affinity, it also would be desirable for the warhead to possess a hydrogen bond acceptor in the vicinity of its electophilic center to accept hydrogen bonds from both catalytic histidines.

■ CONCLUSIONS

KasA, which belongs to the FAS II system in the biosynthetic pathway of the cell wall, is an attractive drug target against tuberculosis because of its pivotal role in the survival of *M. tuberculosis*. Various mechanisms for its catalytic cycle that mainly differ in the assumed protonation state were proposed. The uncertainties arise because information about the real protonation states is difficult to determine by X-ray measurements in this case. To shed some light on this important issue, we characterized variations in the protonation state of the active site along the enzymatic reaction using various theoretical approaches ranging from first-principles-based QM/MM MD simulations to force field-based MD and FEP computations.

Our computational results give answers to three important open questions, e.g., the protonation pattern of the active site in the resting state, the recovery of the enzyme at the end of the catalytic cycle, and the activation of the enzyme at the beginning of the catalytic cycle. According to our new computations, the enzyme takes the neutral protonation pattern (Scheme 2) in its resting state. The description of the electronic structure of the Lys340/Glu354 pair and the usage of appropriate theoretical approaches for the QM part are central to this finding. In contrast to the generally accepted assumption that the Lys340/Glu354 pair forms a stable salt bridge, the new simulations show frequent proton hopping between constituent residues, meaning that the electronic character of the pair can vary between a salt bridge and neutral state. The calculations also predict that, with regard to the Cys171/His311 pair, the neutral state (Scheme 2) is mainly populated (≈90%) in the resting state. However, a population rate of ∼10% for the corresponding zwitterionic state indicates that it is only slightly less stable than the neutral state. A comparison of these results to previous investigations furthermore gives another example that results obtained from pure force field simulations have to be handled with care even if they concern only geometrical parameters.

Our computations can also suggest an answer to the question of how the enzyme recovers at the end of the catalytic cycle. They predict an equilibrium between the neutral and zwitterionic state as well as between the zwitterionic and Cys171(−)/His311(ε) state (Scheme 3). This indicates that, at the end of the catalytic cycle (Scheme 1), which ends in the Cys171(−)/His311(ε) state, the enzyme can recover the protonation pattern of the beginning of the catalytic cycle (neutral) via the zwitterionic state.

The final question concerns the activation of the enzyme at the beginning of the catalytic cycle. This question exists because, in the neutral state, the thiol group of the Cys171 was found to be too unreactive to attack a carbonyl group. A successful attack is possible only through the thiolate group of a deprotonated Cys171 residue that is, for example, present in the zwitterionic state. Combining new computational simulations and structural information about the distribution of polar and nonpolar residues from X-ray crystal structure, this

paper could develop a possible model for the activation. The analysis of the X-ray structures shows that hydrophobic and hydrophilic residues in the malonyl binding pocket are distributed in a way that allows a hydrophobic route and a hydrophilic route to the active site to exist (Figure 7). In our model, the Phe404 residue plays a key role. If it is rotated to an open conformation that is ∼6 kcal/mol above the closed state (Figures 4 and 5), the sufficiently reactive zwitterionic state becomes mainly populated. According to our model, the rotation of Phe404 is induced by the substrate when its hydrophobic part enters the malonyl binding pocket through the hydrophobic route (Figure 7). At that stage, the emerging thiolate is still stabilized from a hydrogen bond network, including protonated His311 via Wat1, His345, and the backbone amides of Cys171 and Phe404. The final activation of the enzyme happens when this hydrogen bond network is destroyed by the hydrophilic part of the substrate that enters the malonyl binding pocket via the hydrophilic route. Through this destruction, the thiolate gains its full reactivity and can successfully attack the carbonyl carbon of the substrate. The mechanism nicely explains the high specificity of KasA because it predicts a substrate-induced activation of the enzyme.

■ ASSOCIATED CONTENT

Supporting Information

Histogram analysis for evaluating the convergence of FEP calculations and the QM/MM optimization results for checking the reliability of GAFF in describing the tetrahedral intermediate. This material is available free of charge via the Internet at http://pubs.acs.org.

■ AUTHOR INFORMATION

Corresponding Author

*E-mail: bernd.engels@mail.uni-wuerzburg.de. Phone: (+49) 931 31-85394. Fax: (+49)931-888-5331.

Funding

Financial support by the Deutsche Forschungsgemeinschaft within the framework of the SFB630 "Recognition, Preparation and Functional Analysis of Agents against Infectious Diseases" is gratefully acknowledged.

Notes

The authors declare no competing financial interest.

■ ACKNOWLEDGMENTS

We thank Prof. C. Kisker for fruitful discussions.

■ ABBREVIATIONS

KasA, β-ketoacyl ACP synthase I; QM/MM, quantum mechanical/molecular mechanical; MD, molecular dynamics; FEP, free energy perturbation; TB, tuberculosis; MDR-TB, multi-drug-resistant tuberculosis; XDR-TB, extensively drug-resistant tuberculosis; FAS, fatty acid synthesis; ACP, acyl carrier protein; DFT, density functional theory; GPU, graphics processing unit; RESP, restrained electrostatic potential; GAFF, general AMBER force field; WHAM, weighted histogram analysis method; PMF, potential of mean force.

■ REFERENCES

(1) World Health Organization (2012) Global Tuberculosis Control 2011 (http://www.who.int/tb/publications/global_report/2011/en/) (accessed May 27, 2013).

(2) Jain, A., and Mondal, R. (2008) Extensively Drug-Resistant Tuberculosis: Current Challenges and Threats. *FEMS Immunol. Med. Microbiol. 53*, 145−150.

(3) Shenoi, S., and Friedland, G. (2009) Extensively Drug-Resistant Tuberculosis: A New Face to an Old Pathogen. *Annu. Rev. Med. 60*, 307−320.

(4) Dubnau, E., Chan, J., Raynaud, C., Mohan, V. P., Lanéelle, M., Yu, K., Quémard, A., Smith, I., and Daffé, M. (2000) Oxygenated Mycolic Acids Are Necessary for Virulence of Mycobacterium Tuberculosis in Mice. *Mol. Microbiol. 36*, 630−637.

(5) Glickman, M. S., Cox, J. S., and Jacobs, W. R., Jr. (2000) A Novel Mycolic Acid Cyclopropane Synthetase Is Required for Cording, Persistence, and Virulence of *Mycobacterium tuberculosis*. *Mol. Cell 5*, 717−727.

(6) Ojha, A., Anand, M., Bhatt, A., Kremer, L., Jacobs, W. R., Jr., and Hatfull, G. F. (2005) GroEL1: A Dedicated Chaperone Involved in Mycolic Acid Biosynthesis during Biofilm Formation in Mycobacteria. *Cell 123*, 861−873.

(7) Bhatt, A., Fujiwara, N., Bhatt, K., Gurcha, S. S., Kremer, L., Chen, B., Chan, J., Porcelli, S. A., Kobayashi, K., Besra, G. S., et al. (2007) Deletion of kasB in *Mycobacterium tuberculosis* Causes Loss of Acid-Fastness and Subclinical Latent Tuberculosis in Immunocompetent Mice. *Proc. Natl. Acad. Sci. U.S.A. 104*, 5157−5162.

(8) Glickman, M. S., and Jacobs, W. R. (2001) Microbial Pathogenesis of *Mycobacterium tuberculosis*: Dawn of a Discipline. *Cell 104*, 477−485.

(9) Daffé, M., and Draper, P. (1998) The Envelope Layers of Mycobacteria with Reference to Their Pathogenicity. *Adv. Microb. Physiol. 39*, 131−203.

(10) Yuan, Y., Zhu, Y., Crane, D. D., and Barry, C. E., III (1998) The Effect of Oxygenated Mycolic Acid Composition on Cell Wall Function and Macrophage Growth in *Mycobacterium tuberculosis*. *Mol. Microbiol. 29*, 1449−1458.

(11) Smith, S., Witkowski, A., and Joshi, A. K. (2003) Structural and Functional Organization of the Animal Fatty Acid Synthase. *Prog. Lipid Res. 42*, 289−317.

(12) Lu, Y.-J., Zhang, Y.-M., and Rock, C. O. (2004) Product Diversity and Regulation of Type II Fatty Acid Synthases. *Biochem. Cell Biol. 82*, 145−155.

(13) Kremer, L., Dover, L. G., Carrère, S., Nampoothiri, K. M., Lesjean, S., Brown, A. K., Brennan, P. J., Minnikin, D. E., Locht, C., and Besra, G. S. (2002) Mycolic Acid Biosynthesis and Enzymic Characterization of the β-Ketoacyl-ACP Synthase A-Condensing Enzyme from *Mycobacterium tuberculosis*. *Biochem. J. 364*, 423−430.

(14) Bhatt, A., Kremer, L., Dai, A. Z., Sacchettini, J. C., and Jacobs, W. R. (2005) Conditional Depletion of KasA, a Key Enzyme of Mycolic Acid Biosynthesis, Leads to Mycobacterial Cell Lysis. *J. Bacteriol. 187*, 7596−7606.

(15) Huang, W., Jia, J., Edwards, P., Dehesh, K., Schneider, G., and Lindqvist, Y. (1998) Crystal Structure of β-Ketoacyl-Acyl Carrier Protein Synthase II from *E. coli* Reveals the Molecular Architecture of Condensing Enzymes. *EMBO J. 17*, 1183−1191.

(16) Luckner, S. R., Machutta, C. A., Tonge, P. J., and Kisker, C. (2009) Crystal Structures of *Mycobacterium tuberculosis* KasA Show Mode of Action within Cell Wall Biosynthesis and Its Inhibition by Thiolactomycin. *Structure 17*, 1004−1013.

(17) Wang, J., Soisson, S. M., Young, K., Shoop, W., Kodali, S., Galgoci, A., Painter, R., Parthasarathy, G., Tang, Y. S., Cummings, R., et al. (2006) Platensimycin Is a Selective FabF Inhibitor with Potent Antibiotic Properties. *Nature 441*, 358−361.

(18) Price, A. C., Rock, C. O., and White, S. W. (2003) The 1.3-Angstrom-Resolution Crystal Structure of β-Ketoacyl-Acyl Carrier Protein Synthase II from *Streptococcus pneumoniae*. *J. Bacteriol. 185*, 4136−4143.

(19) White, S. W., Zheng, J., Zhang, Y.-M., and Rock, C. O. (2005) The Structural Biology of Type II Fatty Acid Biosynthesis. *Annu. Rev. Biochem. 74*, 791−831.

(20) Von Wettstein-Knowles, P., Olsen, J. G., McGuire, K. A., and Henriksen, A. (2006) Fatty Acid Synthesis. Role of Active Site

Histidines and Lysine in Cys-His-His-Type β-Ketoacyl-Acyl Carrier Protein Synthases. *FEBS J. 273*, 695−710.
(21) Moche, M., Dehesh, K., Edwards, P., and Lindqvist, Y. (2001) The Crystal Structure of β-Ketoacyl-Acyl Carrier Protein Synthase II from *Synechocystis* sp. at 1.54 Å Resolution and Its Relationship to Other Condensing Enzymes. *J. Mol. Biol. 305*, 491−503.
(22) Witkowski, A., Joshi, A. K., and Smith, S. (2002) Mechanism of the β-Ketoacyl Synthase Reaction Catalyzed by the Animal Fatty Acid Synthase. *Biochemistry 41*, 10877−10887.
(23) Zhang, Y.-M., Hurlbert, J., White, S. W., and Rock, C. O. (2006) Roles of the Active Site Water, Histidine 303, and Phenylalanine 396 in the Catalytic Mechanism of the Elongation Condensing Enzyme of *Streptococcus pneumoniae*. *J. Biol. Chem. 281*, 17390−17399.
(24) McGuire, K. A., Siggaard-Andersen, M., Bangera, M. G., Olsen, J. G., and von Wettstein-Knowles, P. (2001) β-Ketoacyl-[Acyl Carrier Protein] Synthase I of *Escherichia coli*: Aspects of the Condensation Mechanism Revealed by Analyses of Mutations in the Active Site Pocket. *Biochemistry 40*, 9836−9845.
(25) Lee, W., Luckner, S. R., Kisker, C., Tonge, P. J., and Engels, B. (2011) Elucidation of the Protonation States of the Catalytic Residues in mtKasA: Implications for Inhibitor Design. *Biochemistry 50*, 5743−5756.
(26) Lee, W., and Engels, B. (2013) Clarification on the Decarboxylation Mechanism in KasA Based on the Protonation State of Key Residues in the Acyl-Enzyme State. *J. Phys. Chem. B 117*, 8095−8104.
(27) Paasche, A., Schiller, M., Schirmeister, T., and Engels, B. (2010) Mechanistic Study of the Reaction of Thiol-Containing Enzymes with A,β-Unsaturated Carbonyl Substrates by Computation and Chemoassays. *ChemMedChem 5*, 869−880.
(28) Paasche, A., Schirmeister, T., and Engels, B. (2013) Benchmark Study for the Cysteine−Histidine Proton Transfer Reaction in a Protein Environment: Gas Phase, COSMO, QM/MM Approaches. *J. Chem. Theory Comput. 9*, 1765−1777.
(29) Ufimtsev, I. S., and Martinez, T. J. (2009) Quantum Chemistry on Graphical Processing Units. 3. Analytical Energy Gradients, Geometry Optimization, and First Principles Molecular Dynamics. *J. Chem. Theory Comput. 5*, 2619−2628.
(30) Isborn, C. M., Götz, A. W., Clark, M. A., Walker, R. C., and Martínez, T. J. (2012) Electronic Absorption Spectra from MM and Ab Initio QM/MM Molecular Dynamics: Environmental Effects on the Absorption Spectrum of Photoactive Yellow Protein. *J. Chem. Theory Comput. 8*, 5092−5106.
(31) Jorgensen, W. L., Chandrasekhar, J., Madura, J. D., Impey, R. W., and Klein, M. L. (1983) Comparison of Simple Potential Functions for Simulating Liquid Water. *J. Chem. Phys. 79*, 926.
(32) Case, D., Darden, T., Cheatham, T., Simmerling, C., Wang, J., Duke, R., Luo, R., Crowley, M., Walker, R., Zhang, W., et al. (2010) *AMBER 11*, University of California, San Francisco.
(33) Hornak, V., Abel, R., Okur, A., Strockbine, B., Roitberg, A., and Simmerling, C. (2006) Comparison of Multiple Amber Force Fields and Development of Improved Protein Backbone Parameters. *Proteins 65*, 712−725.
(34) Becke, A. D. (1988) Density-Functional Exchange-Energy Approximation with Correct Asymptotic Behavior. *Phys. Rev. A 38*, 3098−3100.
(35) Lee, C., Yang, W., and Parr, R. G. (1988) Development of the Colle-Salvetti Correlation-Energy Formula into a Functional of the Electron Density. *Phys. Rev. B: Condens. Matter Mater. Phys. 37*, 785−789.
(36) Miehlich, B., Savin, A., Stoll, H., and Preuss, H. (1989) Results Obtained with the Correlation Energy Density Functionals of Becke and Lee, Yang and Parr. *Chem. Phys. Lett. 157*, 200−206.
(37) Frisch, M. J., Pople, J. A., and Binkley, J. S. (1984) Self-Consistent Molecular Orbital Methods. 25. Supplementary Functions for Gaussian Basis Sets. *J. Chem. Phys. 80*, 3265−3269.
(38) Hehre, W. J., Ditchfield, R., and Pople, J. A. (1972) Self-Consistent Molecular Orbital Methods. XII. Further Extensions of Gaussian-Type Basis Sets for Use in Molecular Orbital Studies of Organic Molecules. *J. Chem. Phys. 56*, 2257−2261.
(39) Ditchfield, R., Hehre, W., and Pople, J. (1971) Self-Consistent Molecular-Orbital Methods. IX. An Extended Gaussian-Type Basis for Molecular-Orbital Studies of Organic Molecules. *J. Chem. Phys. 54*, 724−728.
(40) Hariharan, P. C., and Pople, J. A. (1973) The Influence of Polarization Functions on Molecular Orbital Hydrogenation Energies. *Theor. Chim. Acta 28*, 213−222.
(41) Grimme, S., Antony, J., Ehrlich, S., and Krieg, H. (2010) A Consistent and Accurate Ab Initio Parametrization of Density Functional Dispersion Correction (DFT-D) for the 94 Elements H-Pu. *J. Chem. Phys. 132*, 154104.
(42) Furmanchuk, A., Isayev, O., Gorb, L., Shishkin, O. V., Hovorun, D. M., and Leszczynski, J. (2011) Novel View on the Mechanism of Water-Assisted Proton Transfer in the DNA Bases: Bulk Water Hydration. *Phys. Chem. Chem. Phys. 13*, 4311−4317.
(43) Leenders, E. J. M., Guidoni, L., Röthlisberger, U., Vreede, J., Bolhuis, P. G., and Meijer, E. J. (2007) Protonation of the Chromophore in the Photoactive Yellow Protein. *J. Phys. Chem. B 111*, 3765−3773.
(44) Leung, K., and Rempe, S. B. (2005) Ab Initio Molecular Dynamics Study of Glycine Intramolecular Proton Transfer in Water. *J. Chem. Phys. 122*, 184506.
(45) Li, G.-S., Maigret, B., Rinaldi, D., and Ruiz-López, M. F. (1998) Influence of Environment on Proton-Transfer Mechanisms in Model Triads from Theoretical Calculations. *J. Comput. Chem. 19*, 1675−1688.
(46) Liang, X., Montoya, A., and Haynes, B. S. (2011) Local Site Selectivity and Conformational Structures in the Glycosidic Bond Scission of Cellobiose. *J. Phys. Chem. B 115*, 10682−10691.
(47) Mangold, M., Rolland, L., Costanzo, F., Sprik, M., Sulpizi, M., and Blumberger, J. (2011) Absolute pK_a Values and Solvation Structure of Amino Acids from Density Functional Based Molecular Dynamics Simulation. *J. Chem. Theory Comput. 7*, 1951−1961.
(48) Pluhařová, E., Marsalek, O., Schmidt, B., and Jungwirth, P. (2012) Peptide Salt Bridge Stability: From Gas Phase via Microhydration to Bulk Water Simulations. *J. Chem. Phys. 137*, 185101.
(49) Xiao, S., Wang, L., Liu, Y., Lin, X., and Liang, H. (2012) Theoretical Investigation of the Proton Transfer Mechanism in Guanine-Cytosine and Adenine-Thymine Base Pairs. *J. Chem. Phys. 137*, 195101.
(50) Xie, H., Jin, L., Rudić, S., Simons, J. P., and Gerber, R. B. (2012) Computational Studies of Protonated β-D-Galactose and Its Hydrated Complex: Structures, Interactions, Proton Transfer Dynamics, and Spectroscopy. *J. Phys. Chem. B 116*, 4851−4859.
(51) Klamt, A., and Schuerrmann, G. (1993) COSMO: A New Approach to Dielectric Screening in Solvents with Explicit Expressions for the Screening Energy and Its Gradient. *J. Chem. Soc., Perkin Trans. 2*, 799.
(52) *TURBOMOLE*, version 6.1 2009, a development of University of Karlsruhe and Forschungszentrum Karlsruhe GmbH, 1989−2007, TURBOMOLE GmbH, since 2007; available from http://www.turbomole.com. http://www.cosmologic.de/data/DOK_HTML/node5.html (accessed April 27, 2011).
(53) Schaftenaar, G., and Noordik, J. H. (2000) Molden: A Pre- and Post-Processing Program for Molecular and Electronic Structures. *J. Comput.-Aided Mol. Des. 14*, 123−134.
(54) Frisch, M., Trucks, G., Schlegel, H., Scuseria, G., Robb, M., Cheeseman, J., Montgomery, J. A., Jr., Vreven, T., Kudin, K., Burant, J., et al. (2003) *Gaussian 03*, revision C.02, Gaussian Inc., Wallingford, CT.
(55) Bayly, C. I., Cieplak, P., Cornell, W., and Kollman, P. A. (1993) A Well-Behaved Electrostatic Potential Based Method Using Charge Restraints for Deriving Atomic Charges: The RESP Model. *J. Phys. Chem. 97*, 10269−10280.
(56) Wang, J., Wolf, R. M., Caldwell, J. W., Kollman, P. A., and Case, D. A. (2004) Development and Testing of a General Amber Force Field. *J. Comput. Chem. 25*, 1157−1174.

(57) Wang, J., Wang, W., Kollman, P. A., and Case, D. A. (2006) Automatic Atom Type and Bond Type Perception in Molecular Mechanical Calculations. *J. Mol. Graphics Modell. 25*, 247−260.
(58) Zwanzig, R. W. (1955) High-Temperature Equation of State by a Perturbation Method. II. Polar Gases. *J. Chem. Phys. 23*, 1915.
(59) Phillips, J. C., Braun, R., Wang, W., Gumbart, J., Tajkhorshid, E., Villa, E., Chipot, C., Skeel, R. D., Kalé, L., and Schulten, K. (2005) Scalable Molecular Dynamics with NAMD. *J. Comput. Chem. 26*, 1781−1802.
(60) MacKerell, A. D., Jr., Bashford, D., Bellott, M., Dunbrack, R. L., Jr., Evanseck, J. D., Field, M. J., Fischer, S., Gao, J., Guo, H., Ha, S., et al. (1998) All-Atom Empirical Potential for Molecular Modeling and Dynamics Studies of Proteins. *J. Phys. Chem. B 102*, 3586−3616.
(61) Mackerell, A. D., Jr., Feig, M., and Brooks, C. L., III (2004) Extending the Treatment of Backbone Energetics in Protein Force Fields: Limitations of Gas-Phase Quantum Mechanics in Reproducing Protein Conformational Distributions in Molecular Dynamics Simulations. *J. Comput. Chem. 25*, 1400−1415.
(62) Andersen, H. C. (1983) Rattle: A "Velocity" Version of the Shake Algorithm for Molecular Dynamics Calculations. *J. Comput. Phys. 52*, 24−34.
(63) Pitera, J. W., and van Gunsteren, W. F. (2002) A Comparison of Non-Bonded Scaling Approaches for Free Energy Calculations. *Mol. Simul. 28*, 45−65.
(64) Beutler, T. C., Mark, A. E., van Schaik, R. C., Gerber, P. R., and van Gunsteren, W. F. (1994) Avoiding Singularities and Numerical Instabilities in Free Energy Calculations Based on Molecular Simulations. *Chem. Phys. Lett. 222*, 529−539.
(65) Zacharias, M., Straatsma, T. P., and McCammon, J. A. (1994) Separation-Shifted Scaling, a New Scaling Method for Lennard-Jones Interactions in Thermodynamic Integration. *J. Chem. Phys. 100*, 9025−9031.
(66) Lu, N., and Kofke, D. A. (2001) Accuracy of Free-Energy Perturbation Calculations in Molecular Simulation. I. Modeling. *J. Chem. Phys. 114*, 7303.
(67) Lu, N., and Kofke, D. A. (2001) Accuracy of Free-Energy Perturbation Calculations in Molecular Simulation. II. Heuristics. *J. Chem. Phys. 115*, 6866−6875.
(68) Kumar, S., Rosenberg, J. M., Bouzida, D., Swendsen, R. H., and Kollman, P. A. (1992) The Weighted Histogram Analysis Method for Free-Energy Calculations on Biomolecules. I. The Method. *J. Comput. Chem. 13*, 1011−1021.
(69) Ferrenberg, A. M., and Swendsen, R. H. (1988) New Monte Carlo Technique for Studying Phase Transitions. *Phys. Rev. Lett. 61*, 2635−2638.
(70) Souaille, M., and Roux, B. (2001) Extension to the Weighted Histogram Analysis Method: Combining Umbrella Sampling with Free Energy Calculations. *Comput. Phys. Commun. 135*, 40−57.
(71) Grossfield, A. (2013) *WHAM: The Weighted Histogram Analysis Method*, version 2.0.4, (http://membrane.urmc.rochester.edu/content/wham) (accessed May 27, 2013).
(72) Mladenovic, M., Fink, R. F., Thiel, W., Schirmeister, T., and Engels, B. (2008) On the Origin of the Stabilization of the Zwitterionic Resting State of Cysteine Proteases: A Theoretical Study. *J. Am. Chem. Soc. 130*, 8696−8705.
(73) Zhang, Y., Kua, J., and McCammon, J. A. (2002) Role of the Catalytic Triad and Oxyanion Hole in Acetylcholinesterase Catalysis: An Ab Initio QM/MM Study. *J. Am. Chem. Soc. 124*, 10572−10577.
(74) Ishida, T., and Kato, S. (2003) Theoretical Perspectives on the Reaction Mechanism of Serine Proteases: The Reaction Free Energy Profiles of the Acylation Process. *J. Am. Chem. Soc. 125*, 12035−12048.
(75) Schaefer, B., Kisker, C., and Sotriffer, C. A. (2011) Molecular Dynamics of *Mycobacterium tuberculosis* KasA: Implications for Inhibitor and Substrate Binding and Consequences for Drug Design. *J. Comput.-Aided Mol. Des. 25*, 1053−1069.